Separation Science and Technology
Publication details, including instructions for authors and subscription information:
http://www.informaworld.com/smpp/title~content=t713708471

Effects of Membrane Parameters on Performance of Vapor Permeation through a Composite Supported Liquid Membrane

Li-Zhi Zhang[a]
[a] Key Laboratory of Enhanced Heat Transfer and Energy Conservation of Education Ministry, School of Chemical and Energy Engineering, South China University of Technology, Guangzhou, China

To cite this Article Zhang, Li-Zhi(2006) 'Effects of Membrane Parameters on Performance of Vapor Permeation through a Composite Supported Liquid Membrane', Separation Science and Technology, 41: 16, 3517 — 3538
To link to this Article: DOI: 10.1080/01496390600998052
URL: http://dx.doi.org/10.1080/01496390600998052

Separation Science and Technology, 41: 3517–3538, 2006

ISSN 0149-6395 print/1520-5754 online
DOI: 10.1080/01496390600998052

Effects of Membrane Parameters on Performance of Vapor Permeation through a Composite Supported Liquid Membrane

Li-Zhi Zhang
Key Laboratory of Enhanced Heat Transfer and Energy Conservation of Education Ministry, School of Chemical and Energy Engineering, South China University of Technology, Guangzhou, China

Abstract: Support liquid membranes have been used in air dehumidification due to their inherent high mass transfer rates. In this study, the effects of membrane structural parameters on vapor permeation through a LiCl solution based supported liquid membrane are investigated. To aid in the analysis, a mass transfer model has been proposed for moisture transfer through the membrane, which is composed of a supported liquid layer sandwiched by two hydrophobic protective layers. The model takes into account of the resistance in boundary layers, in the protective hydrophobic layers, and in the supported liquid layer. It is a transient model. It also reflects the distributed nature of moisture permeation through the membrane. The results found that the emission rate exhibits a non-uniform distribution nature on the membrane surface. The structural parameters of the support and the protective layers, such as thickness, pore diameters, and porosity, have great effects on vapor permeation.

Keywords: Membranes, mass transfer, modelling, separations, air dehumidification, composite liquid membrane

INTRODUCTION

With developments in membrane technology, polymer membranes have been used in air dehumidification. Hydrophilic membranes that are permeable to

Received 23 May 2006, Accepted 29 August 2006
Address correspondence to Li-Zhi Zhang, Key Laboratory of Enhanced Heat Transfer and Energy Conservation of Education Ministry, School of Chemical and Energy Engineering, South China University of Technology, Guangzhou 510640, China. Tel./Fax: +86-20-87114268; E-mail: lzzhang@scut.edu.cn

vapor, but impermeable to air, have been considered. However, moisture diffusion in solid polymer membranes are usually very low, in the order of $10^{-12} \sim 10^{-13}$ m^2/s, which has limited their market penetration.

In contrast to solid membranes, moisture diffusion in liquid membranes ($\sim 10^{-9}$ m^2/s) is several orders higher than in solid membranes. Due to this reason and the inherent high selectivity, in recent years, liquid membranes, mainly in the form of composite support liquid membranes, have been tested in air dehumidification and the results are promising (1, 2).

Besides air dehumidification, liquid membranes have been used in many other applications, such as flue gas desulfurization (3), separation of hydrogen sulfide from gas streams (4), removal of 2-chlorophenol from aqueous solution (5), extraction of copper from waste water (6), solute recovery from ionic liquids (7), to name but a few. In these applications, mathematical modeling has become an efficient tool for performance estimation and parameters optimization (3, 8).

In this study, a LiCl solution based composite support liquid membrane designed for air dehumidification has been prepared. The effects of various membrane properties on the vapor permeation will be the focus of study. To aid in the analysis, a detailed mass transfer model is set up. Numerical results are then used to study the effects of membrane characteristics.

EXPERIMENTAL PROCEDURES

Preparation of the Supported Liquid Membrane

A novel membrane, a composite supported liquid membrane (SLM), which employs LiCl liquid solution immobilized in the pores of a support membrane to facilitate the transport of moisture, is prepared. To protect the SLM, two hydrophobic PVDF (Polyvinylidene Fluoride) layers are prepared on both surfaces of the SLM.

Three types of commercial membranes are obtained from a company. A hydrophilic cellulose acetate (CA) membrane (nominal pore diameter 0.22 μm, thickness 52 μm) is used as the support layer to immobilize the LiCl solution. Two hydrophobic PVDF membranes (nominal pore diameter 0.15 μm, thickness 45 μm) are used as the protective layers.

Under room temperatures, a well-stirred LiCl solution of 35% mass fraction is first prepared in a closed glass bottle. Vacuum degassing is applied for 2–5 hours for the three membranes. Then, the CA membrane is soaked into the LiCl solution. After 2 days, the CA membrane is moved from the solution and placed onto a clean glass plate which is cleaned by alcohol. At this stage, PVC glue is brushed on one surface of the two PVDF membranes, and on both surfaces of the CA membrane. After drying for a few hours under ambient conditions, the two PVDF membranes are glued to the CA membrane and are pressed together gently for a few seconds. The

prepared composite membrane is placed in a hygrothermostat for another 24 hours, before the experiments are performed.

Test Rig

A test is conducted to measure the moisture transfer through the composite membrane. It is modified from a stand filed and laboratory emission cell (9). The membrane module is a circular cell with an exchange area of 176.7 cm^2. It is composed of two parts: the lower chamber and the cap, as shown in Fig. 1. During the test, the flat sheet membrane is placed on the lower chamber, inside which a saturated salt solution is added. The cap is then covered on the membrane surface and forms a permeation cell. The membrane and the inner surface of the cap form a flow channel for air. The air is supplied through the air slits in the cap. It is introduced through two diametrically positioned inlets (symmetrically placed) into a circular-shaped channel at the perimeter, from where the air is distributed over the membrane surface through the circular air slit. The air flows inward radially, until it exits the cap outlet in the center. When flowing across the membrane, the air stream exchanges moisture with the salt solution through the composite SLM, and is humidified. This test uses the NaCl solution in its lower chamber since it can ensure outlet humidity not saturated, for the protection of the RH sensors. By monitoring RH changes between the air inlet and outlet, moisture permeation through the composite membrane can be estimated. The humidity and temperature of the flow to and from the cell are measured by the built-in RH and temperature sensors, which are installed in the pumps/controllers.

The whole experimental set-up is shown in Fig. 2. The cell is supplied with clean and humidified air from an air supply unit. The supply air flows from a compressed air bottle and is divided into two streams. One of them is humidified through a bubbler immersed in a bottle of distilled water, and

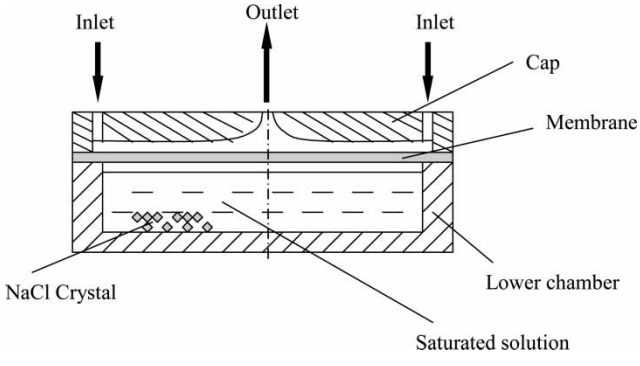

Figure 1. Schematic of the test cell for SLM.

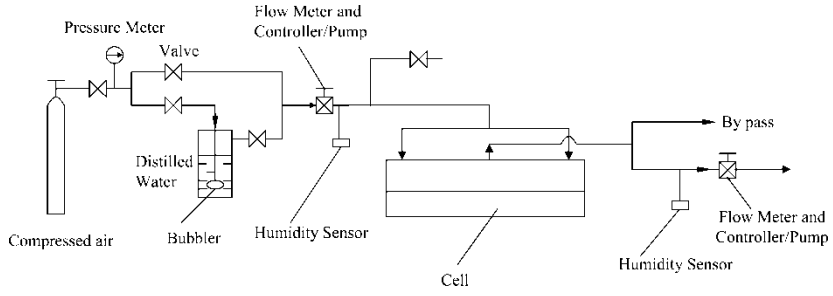

Figure 2. The set-up of the test rig.

it is then re-mixed with the other dry air stream. The humidity of the mixed air stream is controlled by adjusting the proportions of air mixing. The airflow rates are controlled by two air pumps/controllers at the inlet and outlet of the cell.

In the test, the vapor evaporation is slow, and the cell is well conductive. Therefore the whole system is assumed isothermal. The system is a humidification process in fact. However, it can simulate an air dehumidification process. When the NaCl solution in the lower chamber is replaced by LiCl, LiBr, or other salt solution with low saturation vapor pressure, the air will be dehumidified.

MATHEMATICAL MODEL

Moisture Conservation in Air Stream

The schematic of the moisture transport in the cell is represented in Fig. 3. The variations of air humidity are depicted in Fig. 4. The representations are: 1–2, from the lower chamber solution surface to the membrane lower surface; 2–3, from first layer's (PVDF) lower surface to its upper surface;

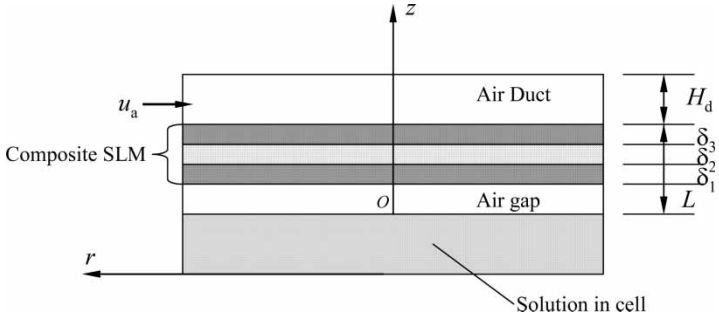

Figure 3. Schematic of the mass transfer model in the cell.

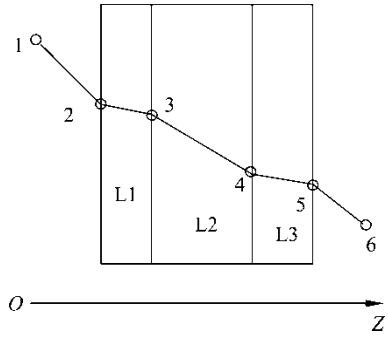

Figure 4. Air humidity variations through the composite membrane.

3–4, from the second layer's (liquid layer) lower surface to its upper surface; 4–5, from the third layer's (PVDF) lower surface to its upper surface; 5–6, from membrane upper surface to air stream.

Moisture conservation in the air stream is represented by a one-dimensional transient equation:

$$\frac{\partial \omega_6}{\partial t} + u_a \frac{\partial \omega_6}{\partial r} = \frac{1}{r}\frac{\partial}{\partial r}\left(D_{va} r \frac{\partial \omega_6}{\partial r}\right) + \frac{J}{H_d \rho_a} \tag{1}$$

where ω_6 is humidity in air stream (kg/kg), t is time (s), r is radius (m), D_{va} is vapor diffusivity in air (m^2/s), u_a is air velocity (m/s) in radial direction, J is the local moisture emission rate from the membrane to air ($kgm^{-2}\,s^{-1}$), H_d is height of air stream at inlet (m), ρ_a is density of dry air (kg/m^3). The upper cavity of the cell is specially designed that the radial air velocity u_a keeps constant in the flow. The air duct height H_d changes with flow.

On the membrane upper surface, the moisture emission rate

$$J = k\rho_a(\omega_5 - \omega_6) \tag{2}$$

where k is the local convective mass transfer coefficient (m/s) between the air stream and the membrane. The convective mass transport in the channel can be represented by (10)

$$Sh = 0.3359\ Re\ Sc\left(\frac{r_0 - r}{2H_d}\right)^{-0.834} \tag{3}$$

where Sh, Re, and Sc are Sherwood number, Reynolds number, and Schmidt

number, respectively. They are defined as

$$Sh = \frac{2kH_d}{D_{va}} \tag{4}$$

$$Re = \frac{2u_a H_d}{\gamma} \tag{5}$$

$$Sc = \frac{\nu}{D_{va}} \tag{6}$$

where γ is the kinematic viscosity of air (m^2/s), r is radial coordinate (m) and r_0 is the radius of the cell (m).

Initial conditions:

$$t = 0, \quad \omega = \omega_L \tag{7}$$

where ω_L is the humidity ratio determined by the saturated NaCl solution and temperature (kg/kg);

Boundary conditions:

$$r = r_0, \quad \omega = \omega_i \tag{8}$$

$$r = 0, \quad \text{stream outlet} \tag{9}$$

Resistance in this component

$$r_D = \frac{1}{\rho_a k} \tag{10}$$

This resistance is the inverse of convective mass transfer coefficient in air flow side, divided by the density of dry air. It is also called the convective resistance.

Moisture Transfer through the Composite Membrane

Moisture diffusion through the composite membrane is expressed by

$$J = D_e \rho_a \frac{\omega_2 - \omega_5}{\delta_1 + \delta_2 + \delta_3} \tag{11}$$

where D_e is the effective moisture diffusion coefficient in the composite membrane (m^2/s), it is calculated by

$$D_e = \frac{\delta_1 + \delta_2 + \delta_3}{(\delta_1/D_{e1}) + (\delta_2/D_{e2}) + (\delta_3/D_{e3})} \tag{12}$$

where D_{e1}, D_{e2}, D_{e3} are the effective diffusivity in the first layer, second layer, and the third layer of the composite membrane.

Effective Diffusivity in the First and the Third Layer

The two protective layers on both sides of the liquid layer are highly hydrophobic. The established theory of gas diffusion in such membranes considers three mechanisms: Poiseuille flow, ordinary molecular diffusion, and Knudsen diffusion, or a combination of all three of them.

When Kn (ratio of the pore size to the mean free path) ≥ 10, the Knudsen flow is dominant, the Poisseuille mechanism may be neglected. Actually, in most cases for air conditioning industry with microporous membranes, the Knudsen number is larger than 10, and the Poisseuille flow can be neglected, then the flow is considered to be combined Knudsen and ordinary diffusion.

An ordinary diffusion coefficient of a water vapor molecule in air is expressed by (11)

$$D_0 = \frac{C_a T^{1.75}}{P_m (v_v^{1/3} + v_a^{1/3})^2} \sqrt{\frac{1}{M_v} + \frac{1}{M_a}} \tag{13}$$

where $C_a = 3.203 \times 10^{-4}$. The terms v_v and v_a are molecular diffusion volumes and are calculated by summing the atomic contributions (11). M_v and M_a are molecule weight of vapor and air in kg/mol.

Knudsen diffusion coefficient (11)

$$D_K = \frac{d_P}{3} \sqrt{\frac{8RT}{\pi M_v}} \tag{14}$$

where R is gas constant, 8.314 J/(mol K).

The effective diffusivity of combined Knudsen and ordinary flow is (11)

$$D_{KO}^{-1} = (D_K^{-1} + D_O^{-1})^{-1} \tag{15}$$

Effective diffusivity in this layer (11)

$$D_{ei} = \frac{\varepsilon_i}{\tau_i} D_{KO,i}, \quad i = 1, 3 \tag{16}$$

Resistance in these two layers

$$r_{1,3} = \frac{\delta_{1,3}}{\rho_a D_{e1,3}} \tag{17}$$

The resistance through these two layers is called the diffusion resistance, which is calculated by diffusion distance divided by air density and moisture diffusivity in the membrane.

Effective Diffusivity in the Second Layer

This layer is the supported liquid layer. Water transfer in liquid layer is described by (3):

$$J = \frac{\varepsilon_2}{\tau_2} D_{\mathrm{wl}} \frac{\Delta \mathrm{C_w}}{\delta_2} \tag{18}$$

where D_{wl} is water diffusivity in the liquid membrane ($\mathrm{m^2/s}$), ΔC_{w} is the difference of water concentration in the liquid membrane solution ($\mathrm{kg/m^3}$) between the two sides of liquid membrane.

Water vapor partial pressure, temperature, and LiCl solution concentration are governed by a thermodynamic equation (12)

$$\log p_{\mathrm{v}} = A(m) + \frac{B(m)}{T} + \frac{C(m)}{T^2} \tag{19}$$

$$A(m) = A_0 + A_1 m + A_2 m^2 + A_3 m^3 \tag{20}$$

$$B(m) = B_0 + B_1 m + B_2 m^2 + B_3 m^3 \tag{21}$$

$$C(m) = C_0 + C_1 m + C_2 m^2 + C_3 m^3 \tag{22}$$

where in this equation p_{v} is in kPa, T is in K, and m is molality of the electrolyte (mol LiCl/kg water).

$$m = \frac{x}{0.0425(1-x)} \tag{23}$$

where x is mass fraction of solute (kg LiCl/kg solution).The constants in equations (19) to (22) are given by (13)

$$\begin{aligned}
&A_0 = 7.3233550, \quad A_1 = -0.0623661,\\
&A_2 = 0.0061613, \quad A_3 = -0.0001042,\\
&B_0 = -1718.1570, \quad B_1 = 8.2255,\\
&B_2 = -2.2131, \quad B_3 = 0.0246,\\
&C_0 = -97575.680, \quad C_1 = 3839.979,\\
&C_2 = -421.429, \quad C_3 = 16.731,
\end{aligned}$$

Water concentration in solution is

$$C_{\mathrm{w}} = (1-x)\rho_{\mathrm{sol}} \tag{24}$$

where ρ_{sol} is solution density ($\mathrm{kg/m^3}$), and it is calculated by the following equation

$$\rho_{\mathrm{sol}} = \rho_{\mathrm{w}} \sum_{i=0}^{3} \rho_{\mathrm{i}} \left(\frac{x}{1-x}\right)^i \tag{25}$$

where ρ_w is pure water density at temperature T, and ρ_i are given below:

$$\rho_0 = 1.0, \quad \rho_1 = 0.540966$$
$$\rho_2 = -0.303792, \quad \rho_3 = 0.100791$$

The humidity ratio in ambient air is in the range of 0.005 kg/kg to 0.035 kg/kg, therefore the above equation can be simplified to

$$p_v = 1.608\omega P \tag{26}$$

The thermodynamic equilibrium chart of LiCl solution dictated by equations (19) to (25) could be represented by a series of linear equations as

$$C_w = k_p p_v + C_{w0} \tag{27}$$

where k_p is called the Henry coefficient ($kgm^{-3}\,Pa^{-1}$), and C_{w0} is a constant (kg/m^3). They are functions of temperature as given in Table 1.

Substituting equation (26) and psychrometric relations into (16) gives the effective moisture diffusivity

$$D_{e2} = \frac{1.608Pk_p\varepsilon_2}{\rho_a\tau_2}D_{wl} \tag{28}$$

Resistance in this layer

$$r_2 = \frac{\delta_2}{\rho_a D_{e2}} \tag{29}$$

As seen, the resistance in this layer is similar to the resistance in the two protective layers. It is calculated by the diffusion distance divided by dry air density and the effective moisture diffusivity in this layer.

Moisture Diffusion in the Air Gap

Moisture transfer below the membrane can be expressed by

$$J = \rho_a D_{va}\frac{\omega_1 - \omega_2}{L} \tag{30}$$

where L is the height of air gap (m).

Table 1. Values of k_p and C_{w0} for LiCl solution

T (°C)	k_p ($kgm^{-3}\,Pa^{-1}$)	C_{w0} (kgm^{-3})
15	0.1434	727.8
25	0.0865	706.4
35	0.0493	700.2
45	0.0293	693.2

Resistance in this component

$$r_{\mathrm{L}} = \frac{\delta_{\mathrm{L}}}{\rho_{\mathrm{a}} D_{\mathrm{va}}} \tag{31}$$

It is also calculated by diffusion distance divided by moisture diffucsivity and dry air density.

Equations (11), (12) can be used for calculations of steady state moisture diffusion. In the transient period, however, influences of initial concentrations in the supported liquid layer should be considered, especially when the liquid layer is thick, therefore, water diffusion in the liquid membrane is determined by mass conservation in a control volume

$$1.608 P k_{\mathrm{p}} \varepsilon_2 \frac{\partial \omega}{\partial t} = \rho_{\mathrm{a}} D_{\mathrm{e2}} \frac{\partial^2 \omega}{\partial z^2} \tag{32}$$

where the term in the left is the change of water quantities in the control volume, and the term in the right is the water influx to the control volume. The two boundary conditions at surfaces:

$$-\rho_{\mathrm{a}} D_{\mathrm{e2}} \left.\frac{\partial \omega}{\partial z}\right|_{z=\delta 2} = \frac{\omega - \omega_6}{r_3 + r_D} \tag{33}$$

$$-\rho_{\mathrm{a}} D_{\mathrm{e2}} \left.\frac{\partial \omega}{\partial z}\right|_{z=\delta 1} = \frac{\omega_1 - \omega}{r_{\mathrm{L}} + r_1} \tag{34}$$

Transient moisture emission rate from the membrane to air stream

$$J = -\rho_{\mathrm{a}} D_{\mathrm{e2}} \left.\frac{\partial \omega}{\partial z}\right|_{z=\delta 2} \tag{35}$$

With equations (32)–(35), transient non-equilibrium distribution of water concentration in the liquid layer can be estimated.

Moisture Permeability

Mean moisture permeability across the whole membrane surface, $(\mathrm{kgm}^{-1}\,\mathrm{s}^{-1})/(\mathrm{kg/kg})$, is calculated by

$$Pe = \frac{u_{\mathrm{a}} \rho_{\mathrm{a}} A_{\mathrm{c}} (\omega_{\mathrm{O}} - \omega_{\mathrm{i}})}{A_{\mathrm{t}} \Delta \omega_{\mathrm{lm}}} (\delta_1 + \delta_2 + \delta_3) \tag{36}$$

where A_{c} is the cross section area of air duct (m^2), A_{t} is the transfer area of membrane in the cell (m^2), $\Delta\omega_{\mathrm{lm}}$ is the logarithmic mean humidity difference between the solution surface and air stream, and it is calculated by

$$\Delta \omega_{\mathrm{lm}} = \frac{\omega_{\mathrm{o}} - \omega_{\mathrm{i}}}{\ln(\omega_{\mathrm{L}} - \omega_{\mathrm{i}} / \omega_{\mathrm{L}} - \omega_{\mathrm{o}})} \tag{37}$$

where subscripts o, i represent the outlet and the inlet of the air stream, respectively.

The permeability *Pe* here represents moisture transfer rate (kg/s) for unit area of membrane under unit transmembrane humidity difference (kg vapor/kg dry air), times total thickness. It reflects the performance of the membrane.

Dimensionless radius

$$r^* = 1 - \frac{r}{r_0} \tag{38}$$

In the simulations, it is assumed that heat effects are negligible due to slow water evaporation rates from the solution. Further, the physical properties like moisture diffusivity are uniform and constant in the membrane.

RESULTS AND DISCUSSION

Non-uniform Transient Character

Both experimental and numerical values of outlet RH are obtained. Table 2 lists the values of operating conditions and system configurations. The tested mean permeation rate across the whole membrane surface is $1.1 \times 10^{-4}\,\mathrm{kgm^{-2}\,s^{-1}}$, which is 3 times higher than the value obtained with a highly hydrophilic solid polymer membrane of comparable thickness ($2.5 \times 10^{-5}\,\mathrm{kgm^{-2}\,s^{-1}}$) (14). The corresponding permeability with this supported liquid membrane is $5.2 \times 10^{-6}\,(\mathrm{kgm^{-1}\,s^{-1}})/(\mathrm{kg/kg})$.

The model provides a tool for system estimation and optimization. To validate the model, the transient lapses of outlet RH with time under different flow rates are depicted in Fig. 5. The discrete dots are the measured values. As can be seen from the figure, some time lag is observed between the measured and the calculated. In fact, in the transient period, measured data is a little bit higher than the model calculations. This is due to the delay of response of RH sensors. Generally speaking, the model

Table 2. Parameters used in the test and analysis

Symbol	Unit	Value	Symbol	Unit	Value
T	°C	26.0	ε_1, ε_3		0.65
δ_1, δ_3	μm	45	ε_2		0.51
δ_2	μm	52	τ_1, τ_3		2.0
d_{p1}, d_{p3}	μm	0.15	τ_2		2.8
d_{p2}	μm	0.22	V	L/min	$10.0 \sim 30$
r_0	mm	75	L	mm	0.1
H_d	mm	1.0			
D_{wl}	m^2/s	(3×10^{-9})			

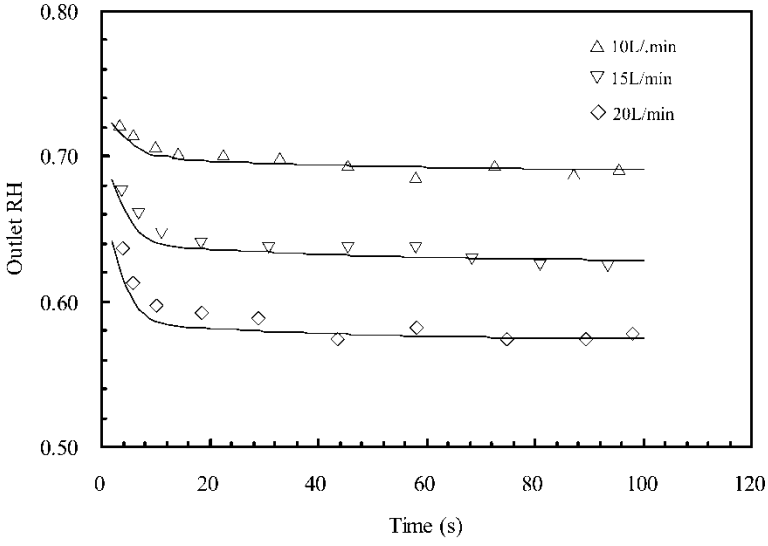

Figure 5. Variations of the outlet RH with lapse of time for different flow rates with the membrane. The discrete dots are experimental data and the solid lines are calculated with the model.

predicts the tested data reasonably well. It takes less than 30 seconds for the moisture transport to becomes steady. After this transient period, stable transport of moisture from the solution to the air stream is established. The greater the air flow rates, the less the outlet RH. The transient responses of outlet RH are mainly influenced by the initial conditions: moisture in the air duct, and water stored in the liquid membrane.

Figure 6 plots the distribution of mass fraction of LiCl (mean in thickness) in the liquid membrane along cell radius, at different time intervals. Before the test, the liquid membrane has a uniform mass fraction of 17.5% which is in equilibrium with salt solution humidity in the lower chamber. During the test, a new equilibrium between the liquid membrane and the air stream humidity has been set up. As a result, LiCl concentration in the liquid membrane re-distributes and forms a non-uniform mass fraction field both in radius and in thickness. Under the gradients of LiCl (or water) concentrations, moisture is transferred from the lower gap to the air stream. The liquid solution layer also acts as a barrier to air transfer since little air can be dissolved in LiCl solution.

Figure 7 shows the local moisture permeation rate along cell radius at different time. As seen, the emission rate exhibits a non-uniform distribution on the membrane surface. In the beginning, the permeation rate is high near air inlet, but it decreases in due course. The reason is that in the beginning, vapor concentration difference between the air stream and the liquid membrane is very large, so a lot of the vapor is evaporated from the membrane surface

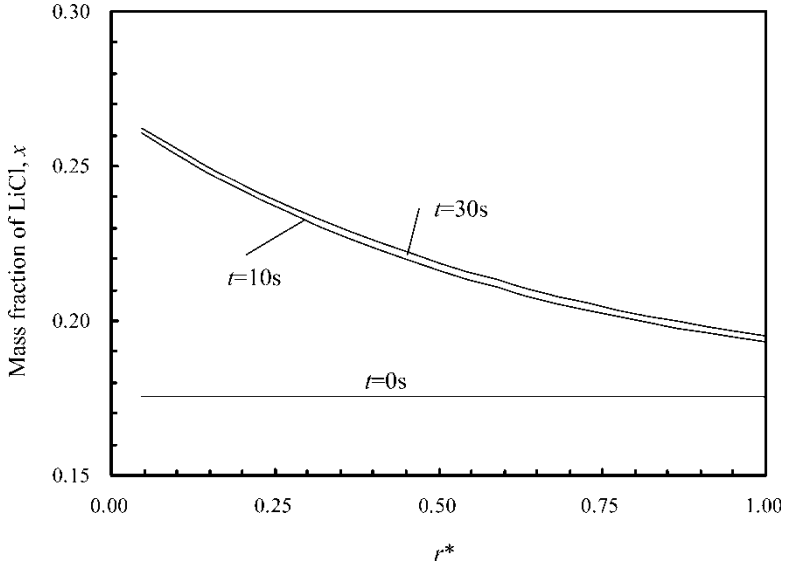

Figure 6. Mean mass fraction of LiCl in liquid layer along cell radius.

to the air stream. However, with time lapse and the new equilibrium setting up, the concentration difference decreases, and the resulting permeation rate decreases to a certain equilibrium value. At the air outlet, the permeation rate changes little with time. These phenomena show the non-uniform transient character of moisture permeation through the composite membrane.

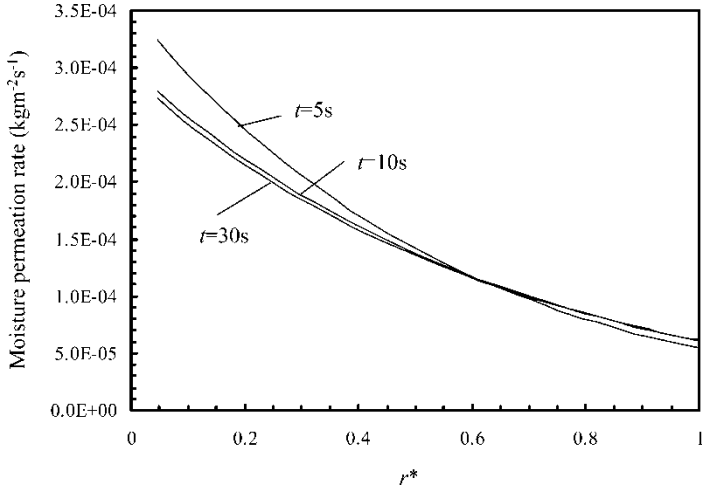

Figure 7. Local moisture permeation rate along cell radius at different time.

Figure 8 shows the percentages of various resistances to total resistance. As seen, the convective moisture transfer resistance accounts for 23% of the total resistance. The two protective layers account for 28% of the total resistance each. The air gap diffusion resistance amounts for less than 10% of the total resistance. The supported liquid layer, LiCl solution layer, only accounts for 12% of the total resistance.

Effects of Protective Layers

The protective layers have great influences on membrane performance. Figure 9 shows the effects of two protective layer thicknesses on mean permeation rate and the permeability through the membrane. The permeation rate decreases with an increase in protective layer thickness, due to the increased moisture resistance. As for the permeability, it first decreases, and then increases with thickness increasing. The reason is that the permeability is co-determined by two contradicting factors: membrane resistance and membrane thickness. The final permeability is the result of the balance between these two factors. When the thickness is less than 20 μm, increased resistance with thickness is more influential, while when the protective thickness is greater than 20 μm, increases of thickness is more influential. When the two protective thicknesses are reduced from 100 μm to 5 μm, the permeation rate can be improved by 20%.

Figure 10 shows the effects of protective layer porosity on the mean permeation rate and the permeability. Porosity plays a big role. Both the permeation rate and the permeability increases with porosity, due to decreased

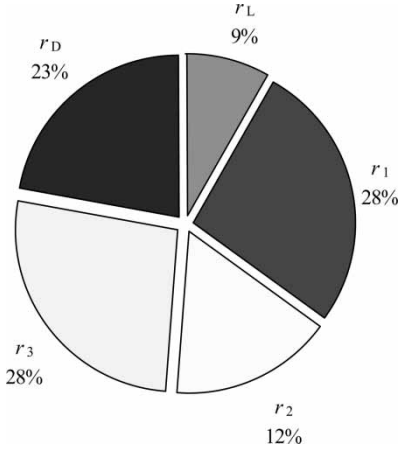

Figure 8. Percentages of various resistances to total moisture transfer resistance.

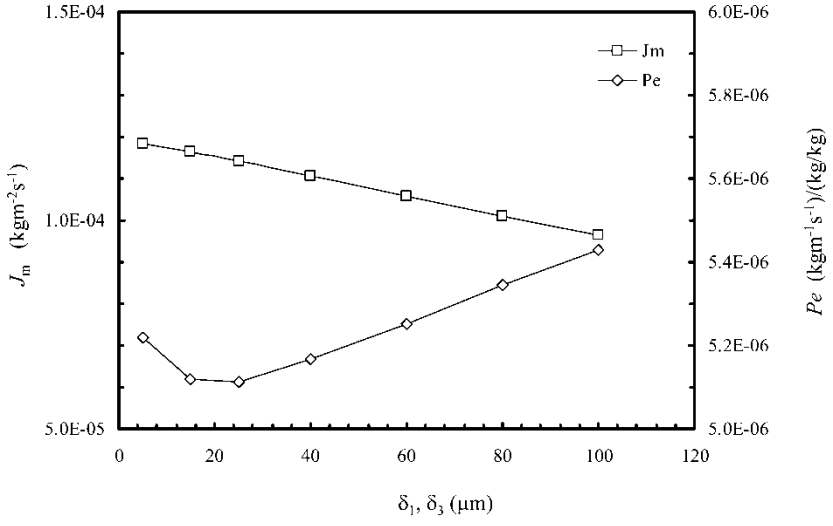

Figure 9. Effects of protective thickness on mean moisture permeation rate and permeability.

resistance. The mean permeation rate increases 1.3 folds with a porosity increase from 0.2 to 0.8.

Figure 11 shows the influence of mean pore diameters of protective layers on performance. The smaller the pore sizes, the greater the resistance, and the

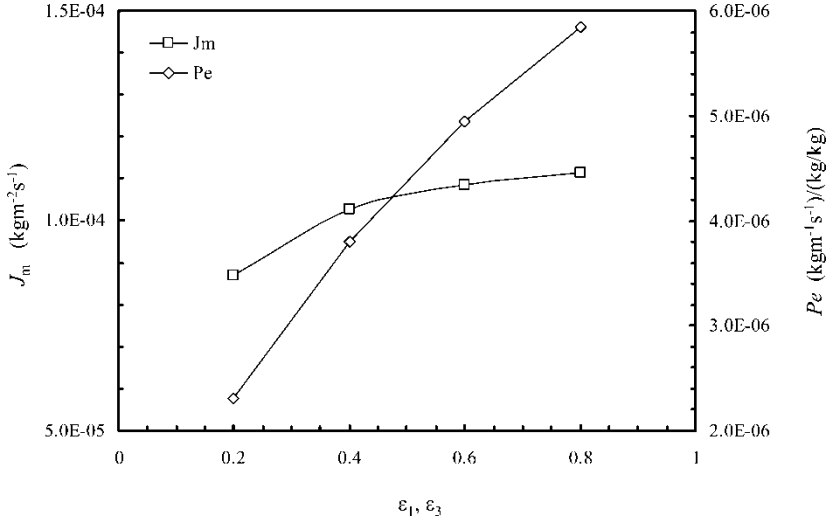

Figure 10. Effects of protective layer porosity on mean permeation rate and permeability.

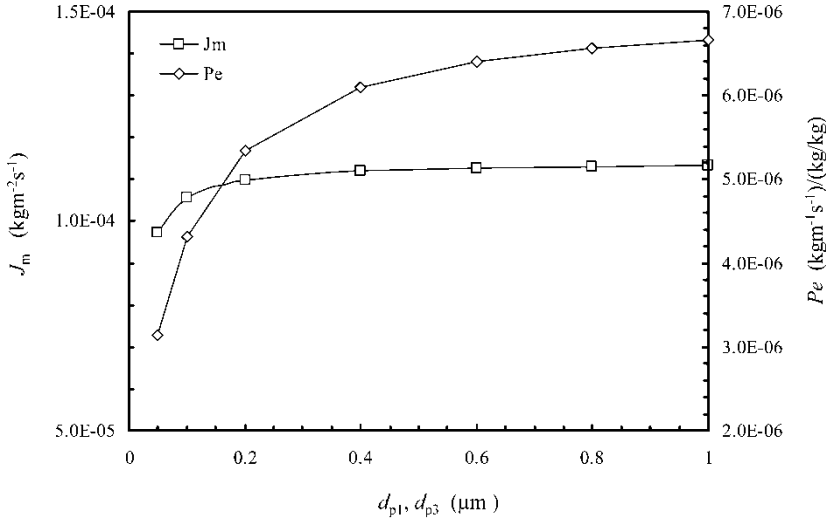

Figure 11. Effects of nominal pore diameter of protective layer on mean permeation rate and permeability.

better the performance. When the pores are greater than 0.4 μm, performance improvement with larger pores becomes slower. On the other hand, with larger pores, the use with protective layers to support and stabilize the liquid layer becomes limited. Therefore a membrane with 0.4 μm diameter pores is a good optimization.

Effects of Liquid Layer

The liquid layer has a major impact on performance, since it is not only the barrier, but also the active layer facilitates moisture transfer. Figures 12 and 13 show the effects of liquid layer thickness and porosity on performances, respectively. As seen, the permeation rate and the permeability decrease with the thickness increasing, due to the resistance increasing. The performance increases with the porosity increasing, due to the resistance decreasing. The porosity has a greater impact on performance than thickness does. An increase of porosity from 0.2 to 0.8 has a 90% permeation rate improvement.

An Application Case

The test set-up symbolizes a passive air dehumidification system. In the air conditioning industry, the contact system is more promising since it has little pressure difference. A fresh air dehumidification system (by exhaust

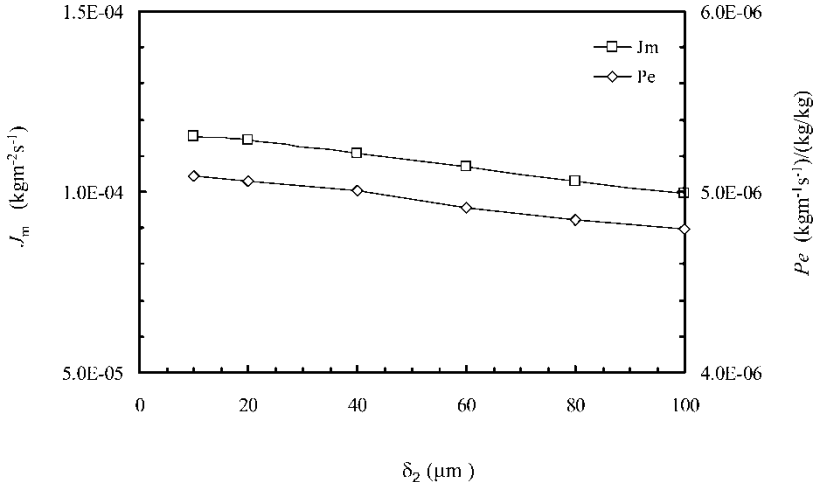

Figure 12. Effects of liquid layer thickness on mean permeation rate and permeability.

air) is shown in Fig. 14. The unit is also called the total heat recovery ventilator. Fresh air (humid air) is dehumidified by exhaust air (dry air) when flowing through membranes.

Hollow fibers are beneficial for vapor permeation, however, pressure resistance will be too high. On the contrary, parallel-plate exchangers, if properly designed, will have good performance, but with much smaller

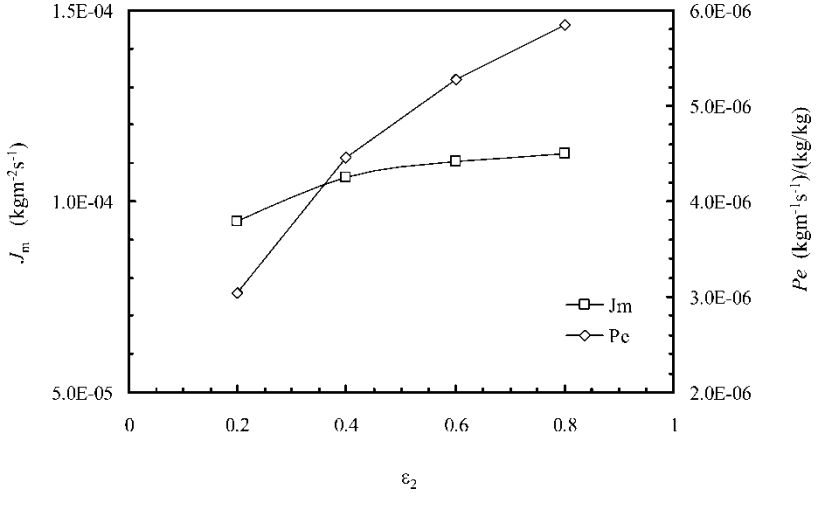

Figure 13. Effects of liquid layer porosity on mean permeation rate and permeability.

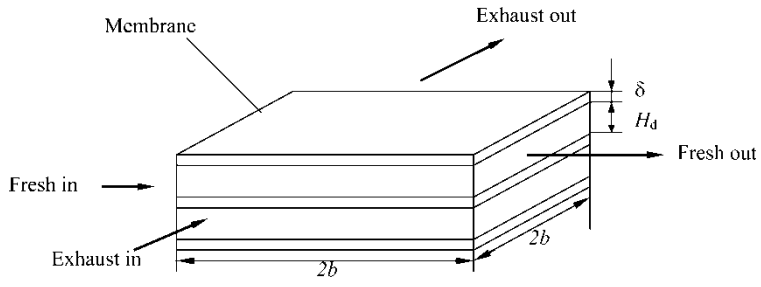

Figure 14. A passive air dehumidification system.

resistance. The design of a parallel-plate membrane total heat exchanger is similar to the design of a sensible heat exchanger. For moisture exchange effectiveness higher than 0.8, the number of transfer units should be greater than 4.2 (15).

$$NTU = \frac{KA_t}{V} \tag{39}$$

where K is total mass transfer coefficient (m/s).

The tested mean permeation rate in this study is

$$J_{\mathrm{m}} = 1.1 \times 10^{-4}\ \mathrm{kgm^{-2}\ s^{-1}}$$

Based on the transfer equation,

$$J_{\mathrm{m}} = K\rho_{\mathrm{a}}\Delta\omega_{\mathrm{lm}}$$

Using the experimental data: Air inlet RH = 20%, Outlet RH = 54%, $V = 20$ L/min, temperature 27°C, RH of the solution surface in the chamber RH = 75%. Correspondingly $\omega_{\mathrm{i}} = 0.0045$ kg/kg; $\omega_{\mathrm{o}} = 0.012$ kg/kg; $\omega_{\mathrm{L}} = 0.017$ kg/kg;

$$\Delta\omega_{\mathrm{lm}} = \frac{(\omega_{\mathrm{L}} - \omega_{\mathrm{i}}) - (\omega_{\mathrm{L}} - \omega_{\mathrm{o}})}{\ln(\omega_{\mathrm{L}} - \omega_{\mathrm{i}}/\omega_{\mathrm{L}} - \omega_{\mathrm{o}})} = 0.0082\ \mathrm{kg/kg}$$

Total mass transfer coefficient in the test

$$K = \frac{J_m}{\rho_a \Delta\omega_{lm}} = \frac{1.1 \times 10^{-4}}{1.2 \times 0.0082} = 0.011\ \mathrm{m/s}$$

In the test, it is estimated that the membrane accounts for 68% of the total resistance, therefore the membrane resistance is

$$r_m = 0.68 r_{tot} = 0.68\frac{1}{K} = 61.8\ \mathrm{s/m}$$

An air ventilator with flow capacity 1000 m^3/h is considered. Duct spacing is selected as 2 mm. For fully developed laminar flow in parallel plate ducts, Sh = 7.54 (16).

Then the convective mass transfer coefficient on both sides of membrane in duct is

$$k = \frac{Sh \cdot D_{va}}{D_h} = \frac{7.54 \times 2.82 \times 10^{-5}}{0.004} = 0.053 \text{ m/s}$$

Then the total resistance in the designed ventilator:

$$r_{tot} = \frac{2}{k} + r_m = 99.5 \text{ s/m}$$

The total mass transfer coefficient

$$K = \frac{1}{r_{tot}} = 0.01 \text{ m/s}$$

As seen, the total mass transfer coefficient is in the same magnitude with those under the test conditions. The membrane is the predominant factor influencing performance, rather than the flow configurations.

To have an effectiveness of 0.80, we must have $NTU = 4.2$, then we need an area of

$$A_t = \frac{V \cdot NTU}{K} = \frac{1000/3600 \times 4.2}{0.01} = 116 \text{ m}^2$$

If a square membrane 1 m long is selected, then the total number of membranes $n = 116/1.0^2 = 116$. The ventilator core's dimension is $1.0 \times 1.0 \times 0.24$ m^3. Both the fresh air and the exhaust have 58 ducts each.

Mean air velocity in ducts

$$u_a = \frac{1000/3600}{58 \times 1.0 \times 0.002} = 2.4 \text{ m/s}$$

Reynolds number

$$Re = \frac{D_h u_a}{\gamma} = \frac{0.004 \times 2.4}{15.89 \times 10^{-6}} = 604$$

Since $Re < 2300$, flow is laminar. Assumption is valid.

According to ASHRAE standard, a 1000 m^3/h ventilator is enough for an office of 350 m^2 floor area, for fresh air supply purposes. For such a unit, an exchange area of 116 m^2 is acceptable. The estimated material cost is 370USD.

Therefore, the parallel-plate membrane exchangers are feasible from both the technical and economical points of view.

CONCLUSIONS

A composite supported liquid membrane for air dehumidification has been developed. A test is done to measure its moisture transfer potential. A transient non-uniform model has been set up to take into account the resistance in the three layers. The results are that:

(1) The mean permeation rate across the membrane is 3 times higher than that through a highly hydrophilic solid polymer membrane of comparable thickness due to facilitated transport.
(2) The model can be used to study the mass transfer mechanisms in the cell. The moisture transfer on membrane surface shows a non-uniform, transient character.
(3) Better performance can be obtained with membrane optimization. Thickness, pore diameters, and porosity can be optimized. The most effective way is to have a high porosity for both the protective layers and the liquid support layer.
(4) A case design shows that a contact passive system is feasible, both technically and economically.

NOMENCLATURE

A	area (m^2)
C	concentration (kg/m^3)
D	diffusivity (m^2/s)
D_h	hydrodynamic diameter (m)
d_p	pore diameter (m)
H_d	duct height at inlet (m)
J	emission rate ($kgm^{-2}\,s^{-1}$)
k	convective mass transfer coefficient (m/s)
Kn	Knudsen number
k_p	Henry constant ($kgm^{-3}\,Pa^{-1}$)
K	total transfer coefficient (m/s)
L	height of air gap (m)
m	molality of electrolyte (mol LiCl/kg water)
M	molecule weight (kg/mol)
NTU	Number of transfer units
p	partial pressure (Pa)
P	total pressure (Pa)
Pe	permeability ($kgm^{-1}\,s^{-1}$)/(kg/kg)
R	gas constant, 8.314 J/(mol K)
r	radius coordinate (m); resistance (m^2s/kg, or s/m)
r_0	cell radius (m)
Sh	Sherwood number

T	temperature (K)
u_a	air bulk velocity along radius (m/s)
V	air flow rate (L/min)
v	molecular diffusion volume
x	mass fraction of solute (kg LiCl/kg solution)

Greek Letters

ϕ	relative humidity
ρ	density (kg/m^3)
ω	humidity ratio (kg moisture/kg air)
γ	kinematic viscosity of air (m^2/s)
τ	pore tortuosity
ε	porosity
δ	thickness (μm)

Superscripts

*	dimensionless

Subscripts

a	air
D	air stream
e	effective
i	inlet
k	Knudsen
l	liquid
L	lower chamber
m	mean
o	outlet, ordinary
sol	solution
v	vapor
W	liquid water

ACKNOWLEDGEMENTS

This Project is jointly supported by National Natural Science Foundation of China (50306005), Fok Ying Tung Education Foundation (101057), and Natural Science Foundation of Guangdong Province (05006557).

REFERENCES

1. Ito, A. (2000) Dehumidification of air by a hygroscopic liquid membrane supported on surface of a hydrophobic microporous membrane. *Journal of Membrane Science*, 175 (1): 35.

2. Kojima, T., Shimizu, H., and Ito, A. (2004) Dehumidification of air using zeolite-filled triethylene glycol liquid membranes. *Journal of the Japan Petroleum Institute*, 47 (6): 403.
3. Sengupta, A., Raghuraman, B., and Sirkar, K.K. (1990) Liquid membranes for flue gas desulfurization. *Journal of Membrane Science*, 51 (1–2): 105.
4. Quinn, R., Appleby, J.B., and Pez, G.P. (2002) Hydrogen sulfide separation from gas streams using salt hydrate chemical absorbents and immobilized liquid membranes. *Separation Science and Technology*, 37 (3): 627.
5. Lin, S.H., Pan, C.L., and Leu, H.G. (2002) Equilibrium and mass transfer characteristics of 2-chlorophenol removal from aqueous solution by liquid membrane. *Chemical Engineering Journal*, 87 (2): 163.
6. Dreher, T.M. and Stevens, G.W. (1998) Instability mechanisms of supported liquid membranes. *Separation Science and Technology*, 33 (6): 835.
7. Fortunato, R., Afonso, C.A.M., Reis, M.A.M., and Crespo, J.G. (2004) Supported liquid membranes using ionic liquids: study of stability and transport mechanisms. *Journal of Membrane Science*, 242 (1–2): 197.
8. Alhusseini, A. and Ajbar, A. (2000) Mass transfer in supported liquid membranes: a rigorous model. *Mathematical and Computer Modeling*, 32 (3–4): 265.
9. Zhang, L.Z. (2006) Evaluation of moisture diffusivity in hydrophilic polymer membranes: a new approach. *Journal of Membrane Science*, 269 (1–2): 75.
10. Zhang, L.Z. and Niu, J.L. (2003) Laminar fluid flow and mass transfer in a standard field and laboratory emission cell (FLEC). *International Journal of Heat Mass Transfer*, 46 (1): 91.
11. Tomaszewska, M., Gryta, M., and Morawski, A.W. (2000) Mass transfer of HCl and H_2O across hydrophobic membrane during membrane distillation. *Journal of Membrane Science*, 166 (2): 149.
12. Patil, K.R., Tripathi, A.D., Pathak, G., and Katti, S.S. (1990) Thermodynamic properties of aqueous electrolyte solutions. 1. vapor pressure of aqueous solutions of LiCl, LiBr, and LiI. *Journal of Chemical Engineering Data*, 35 (2): 166.
13. Conde, M.R. (2004) Properties of aqueous solutions of lithium and calcium chlorides: formulations for use in air conditioning equipment design. *International Journal of Thermal Sciences*, 43 (4): 367.
14. Zhang, L.Z. and Jiang, Y. (1999) Heat and mass transfer in a membrane-based energy recovery ventilator. *Journal of Membrane Science*, 163 (1): 29.
15. Zhang, L.Z. and Niu, J.L. (2002) Effectiveness correlations for heat and moisture transfer processes in an enthalpy exchanger with membrane cores. *ASME Journal of Heat Transfer*, 122 (5): 922.
16. Incropera, F.P. and Dewitt, D.P. (1996) *Introduction to Heat Transfer*; John Wiley and Sons: NewYork.